ADVANCED FUNCTIONAL MATERIALS
www.afm-journal.de

Selective Effects of the Host Matrix in Hydrogenated InGaAsN Alloys: Toward an Integrated Matrix/Defect Engineering Paradigm

Francesco Filippone, Saeed Younis, Giuseppe Mattioli, Marco Felici, Elena Blundo, Antonio Polimeni, Giorgio Pettinari, Damiano Giubertoni, Eduard Sterzer, Kerstin Volz, Dan Fekete, Eli Kapon, and Aldo Amore Bonapasta*

Saeed Younis, one of our co-authors, prematurely passed away while this manuscript was being prepared. This work is dedicated to him.

In dilute nitride $In_yGa_{1-y}As_{1-x}N_x$ alloys, a spatially controlled tuning of the energy gap can be realized by combining the introduction of N atoms—inducing a significant reduction of this parameter—with that of hydrogen atoms, which neutralize the effect of N. In these alloys, hydrogen forms N–H complexes in both Ga-rich and In-rich N environments. Here, photoluminescence measurements and thermal annealing treatments show that, surprisingly, N neutralization by H is significantly inhibited when the number of In-N bonds increases. Density functional theory calculations account for this result and reveal an original, physical phenomenon: only in the In-rich N environment, the $In_yGa_{1-y}As$ host matrix exerts a selective action on the N–H complexes by hindering the formation of the complexes more effective in the N passivation. This thoroughly overturns the usual perspective of defect-engineering by proposing a novel paradigm where a major role pertains to the defect-surrounding matrix.

1. Introduction

Previous studies of hydrogenated dilute-nitride III–V-N alloys focused on two phenomena having remarkable effects on the band gap energy: a significant decrease of the III–V alloy band gap induced by small percentages of N and the partial or full recovery of the N-free alloy band gap induced by atomic hydrogen incorporation.[1–3] Those studies clarified also the central role of the N–H complexes in the N neutralization.[1,4–8] In $GaAs_{1-x}N_x$, H fully neutralizes the effects of N. This phenomenon was exploited for the realization of single-photon emitters using a spatially selective hydrogen incorporation/removal at the sub-micrometer scale, which

F. Filippone, G. Mattioli, A. Amore Bonapasta
ISM-CNR
Istituto di Struttura della Materia –Consiglio Nazionale delle Ricerche
Via Salaria Km 29.5, Monterotondo I-00015, Italy
E-mail: francesco.filippone@cnr.it

S. Younis, M. Felici, E. Blundo, A. Polimeni
Dipartimento di Fisica and CNISM
Sapienza Università di Roma
Piazzale A. Moro 2, Roma I-00185, Italy

G. Pettinari
CNR-IFN
Istituto di Fotonica e Nanotecnologie–Consiglio Nazionale delle Ricerche
Via Cineto Romano, 42, Rome I-00156, Italy

The ORCID identification number(s) for the author(s) of this article can be found under https://doi.org/10.1002/adfm.202108862.

DOI: 10.1002/adfm.202108862

D. Giubertoni
Sensors and Devices
Fondazione Bruno Kessler
Centre for Materials and Microsystems
Micro Nano Facility
Via Sommarive 18, Trento 38123, Italy

E. Sterzer, K. Volz
Department of Physics and Material Sciences Center
Philipps University Marburg
Marburg 35032, Germany

D. Fekete, E. Kapon
Ecole Polytechnique Fédérale de Lausanne (EPFL)
Laboratory of Physics of Nanostructures
Lausanne CH-1015, Switzerland

D. Fekete
Department of Physics
Technion-Israel Institute of Technology
Haifa 32000, Israel

permitted a spatial tuning of the energy gap.[9–11] This approach would be even more interesting in $In_yGa_{1-y}As_{1-x}N_x$, whose band gap energy may be brought in the telecommunication wavelength range.[12] However, indications of an uncertain N passivation in hydrogenated $InAs_{1-x}N_x$[13–15] have prompted the need to understand the conditions that may favor or not such passivation in $In_yGa_{1-y}As_{1-x}N_x$ alloys, where the local N environment ranges from 4Ga-N clusters (encountered in GaAsN) to 4In-N clusters (as it occurs in InAsN). Such an issue has motivated the present study, focused on possible relationships between the cationic environment of N atoms and a different H efficiency in the neutralization of the effects of N. These relationships have been investigated here by combining annealing treatments with photoluminescence (PL) spectroscopy measurements. In this regard, previous studies showed that, in InGaAsN, thermal annealing increases both the number of In-N bonds and the band gap energy.[16–18] Therefore, PL measurements combined with annealing treatments provide a quite reliable method to ascertain the migration of In atoms toward N as well as how the variation of the N environment from a Ga-rich to an In-rich one can affect hydrogen's ability to neutralize the effects of N. Present PL investigations of $In_yGa_{1-y}As_{1-x}N_x$ quantum wells (QWs) show that, for increasing H doses, the alloy band gap energy increases, but it does not reach the corresponding N-free $In_yGa_{1-y}As$ band gap energy. Moreover, the measurement of the dependence of the band gap recovery of hydrogenated InGaAsN on the thermal annealing temperature shows that an In-rich environment for N atoms results in a much lower degree of N passivation. At first glance, this result seems explained by the occurrence of an N environment in the annealed InGaAsN alloy similar to that present in InAsN, which would induce a similar hydrogen behavior. Instead, present Density Functional Theory (DFT) investigations reveal a thoroughly novel phenomenon, fully explaining the experimental findings: in InGaAsN, only in the case of the In-rich N environment, the host InGaAs matrix exerts a selective action on the N–H complexes, by hindering the formation of the most efficient complexes for the N passivation. The increase of In-N clusters is accompanied therefore by a decrease in the number of the most effective N–H complexes and, then, by a reduced neutralization of the N effects. This previously unknown host-matrix effect can induce an evolution from the usual material design protocols toward integrated matrix/defect engineering approaches.

2. Results and Discussion

2.1. Experimental Results

A double QW InGaAsN/InGaAs sample was exposed to a hydrogen ion beam, as sketched in **Figure 1**a. Figure 1b shows the room temperature PL spectra of the pristine and hydrogenated samples for increasing H dose, d_H. We readily notice that the energy of the emission peak of the N-free reference is unchanged with d_H. Instead, a sizable blue-shift of the PL peak of the N-containing QW is observed, indicating N passivation by H. This, in turn, leads to a band gap increase of the InGaAsN material toward the band gap of the N-free host lattice. However, above a given H dose the band gap opening is halted and further H treatments do not cause sizable changes in the PL spectra, see topmost curve in Figure 1b. This is clearly very different with respect to In-free GaAsN, where a full passivation of the N atoms can be achieved.[8]

The most simple and straightfoward explanation of the behavior described in Figure 1b could be related to a different In content in the two QWs; however, secondary ion mass spectrometry (SIMS) measurements rule out such an hypothesis, see Figure 1c.

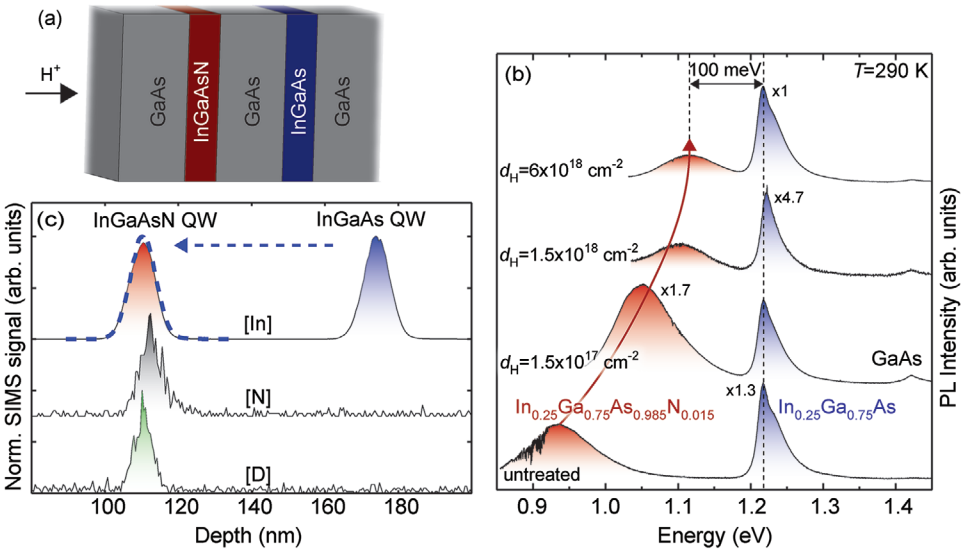

Figure 1. a) Sketch of the sample structure. The sample contains an $In_{0.25}Ga_{0.75}As_{0.985}N_{0.015}$ QW and a reference $In_{0.25}Ga_{0.75}As$ QW, which have an equal thickness of 5.6 nm and are separated by a 50 nm-thick GaAs barrier. b) Room temperature photoluminescence (PL) spectra of the double QW for different H doses, d_H. The PL peaks corresponding to the N-containing and N-free QWs are indicated. c) SIMS depth profile of the deuterated double QW sample. The depth profile of each atomic species is indicated in the figure. The $In_{0.25}Ga_{0.75}As$ In peak has been projected onto the $In_{0.25}Ga_{0.75}As_{0.985}N_{0.015}$ one, as shown by the dashed line, to highlight the very similar In concentrations and thicknesses in the two QWs.

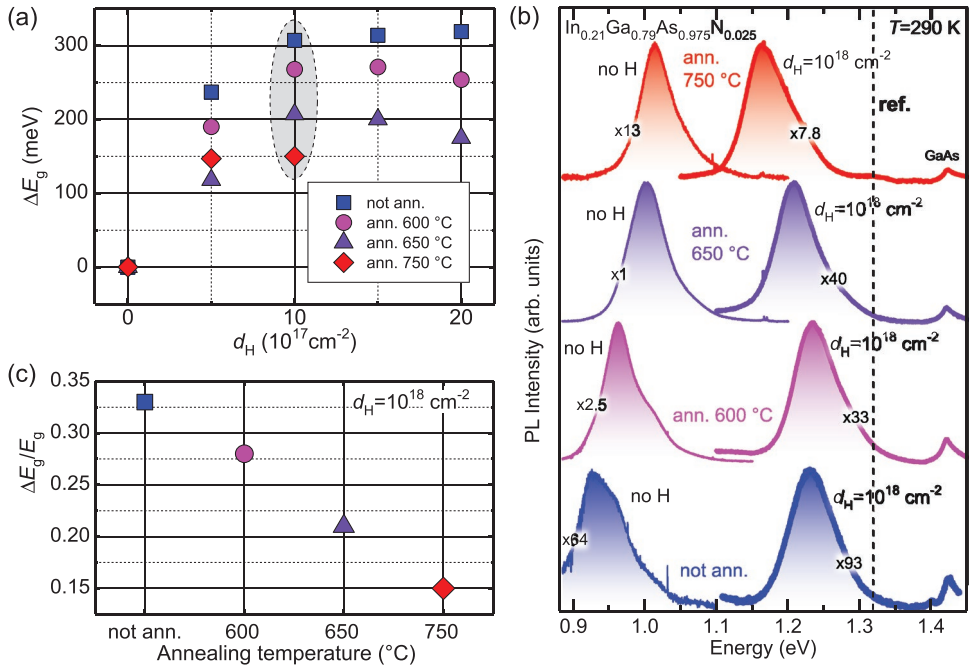

Figure 2. a) Blue-shift of the PL peak energy (ΔE_g) induced by different H doses (d_H) in the $In_{0.21}Ga_{0.79}As_{0.975}N_{0.025}$ QW annealed at 600, 650, and 750 °C, (for 10, 30, and 10 s, respectively), as well as in a nonannealed sample. Notice the saturation of the peak energy for $d_H = 10^{18}$ cm^{-2}. b) Room temperature photoluminescence spectra of the $In_{0.21}Ga_{0.79}As_{0.975}N_{0.025}$ QW for different post-growth annealings (including the not annealed sample, bottom-most spectra) and hydrogenation with a H dose d_H of 10^{18} cm^{-2}. For each annealing, the spectra of the not hydrogenated and of the hydrogenated sample are shown. The vertical dashed line labeled as ref. indicates the QW emission energy of an $In_{0.21}Ga_{0.79}As$ QW. The energy was calculated within the envelope function approximation using the nominal QW parameters. c) $\Delta E_g/E_g$ ratio measured for the same QW of Panel (b) at different annealing temperatures.

The results presented so far indicate that H is significantly less effective at passivating N atoms in In-containing dilute nitrides with respect to the GaAsN case. We will show that this finding is related to the local N environment. Thus, we further investigated this issue by performing a series of thermal annealing treatments on InGaAsN single QWs, which are known to favor the formation of 4In-N clusters in this material.[17]

Figure 2a shows the blue-shift of the PL peak energy (ΔE_g) induced by different H doses (d_H) in samples containing an $In_{0.21}Ga_{0.79}As_{0.975}N_{0.025}$ QW annealed at 600, 650, and 750 °C, as well as not subjected to any thermal treatment. The shift of the PL peak energy saturates at $d_H = 10^{18}$ cm^{-2}, where the maximum band gap recovery is attained for all the investigated samples.

The PL spectra of the three annealed samples irradiated with this H dose are shown in Figure 2b. The bottom-most spectra refer to a nonannealed sample before and after H irradiation. The hydrogenated, not annealed QW shows a blue-shift of the PL peak energy of about ΔE_g = 300 meV. In the annealed samples—thus characterized by an In-richer environment around the N atoms[16–18]—two different behaviors can be observed. First, in the H-free QWs, the PL peak moves at higher energy with increasing annealing temperature, in agreement with the mentioned, previous studies.[16,17] Second, the amount of band gap recovery induced by hydrogenation decreases rapidly with increasing annealing temperature. This latter finding indicates that an In-rich neighborhood inhibits the N atom passivation.

Table 1 and Figure 2c summarize these experimental results. In particular, they report the variation of the $\Delta E_g/E_g$ ratio for different annealing conditions. This quantity depends strongly on the annealing temperature, further strengthening the indication given by the E_g trend in Table 1.

2.2. Theoretical Results

N–H complexes in the $In_{0.21}Ga_{0.79}As_{0.975}N_{0.025}$ alloy were investigated by applying two simplifying assumptions: i) 4Ga-N and 4In-N clusters were considered as representatives of Ga-rich and In-rich N environments, respectively, by disregarding clusters of intermediate composition, and ii) the as-grown and thermally annealed samples of the same alloy were simulated by two "extreme" models, characterized by the presence of 4Ga-N clusters only and 4In-N clusters only, respectively, in an ideal $In_{0.20}Ga_{0.80}As_{0.97}N_{0.03}$ alloy (details in Section S1, Supporting Information).

Table 1. The first row of the Table reports the band gap energies, E_g, estimated by the PL spectra of Figure 2b for the as grown and annealed $In_{0.21}Ga_{0.79}As_{0.975}N_{0.025}$ QWs before hydrogenation. The corresponding E_g values after hydrogenation, differences between the latter and the former E_g values, ΔE_g, and $\Delta E_g/E_g$ ratios are reported in the second, third, and fourth row, respectively.

	AG (as grown)	ANN (600 °C)	ANN (650 °C)	ANN (750 °C)
E_g (InGaAsN) [eV]	0.930	0.962	1.002	1.016
E_g (InGaAsN + H) [eV]	1.231	1.234	1.210	1.163
ΔE_g [eV]	0.301	0.272	0.208	0.147
$\Delta E_g/E_g$	32%	28%	21%	14%

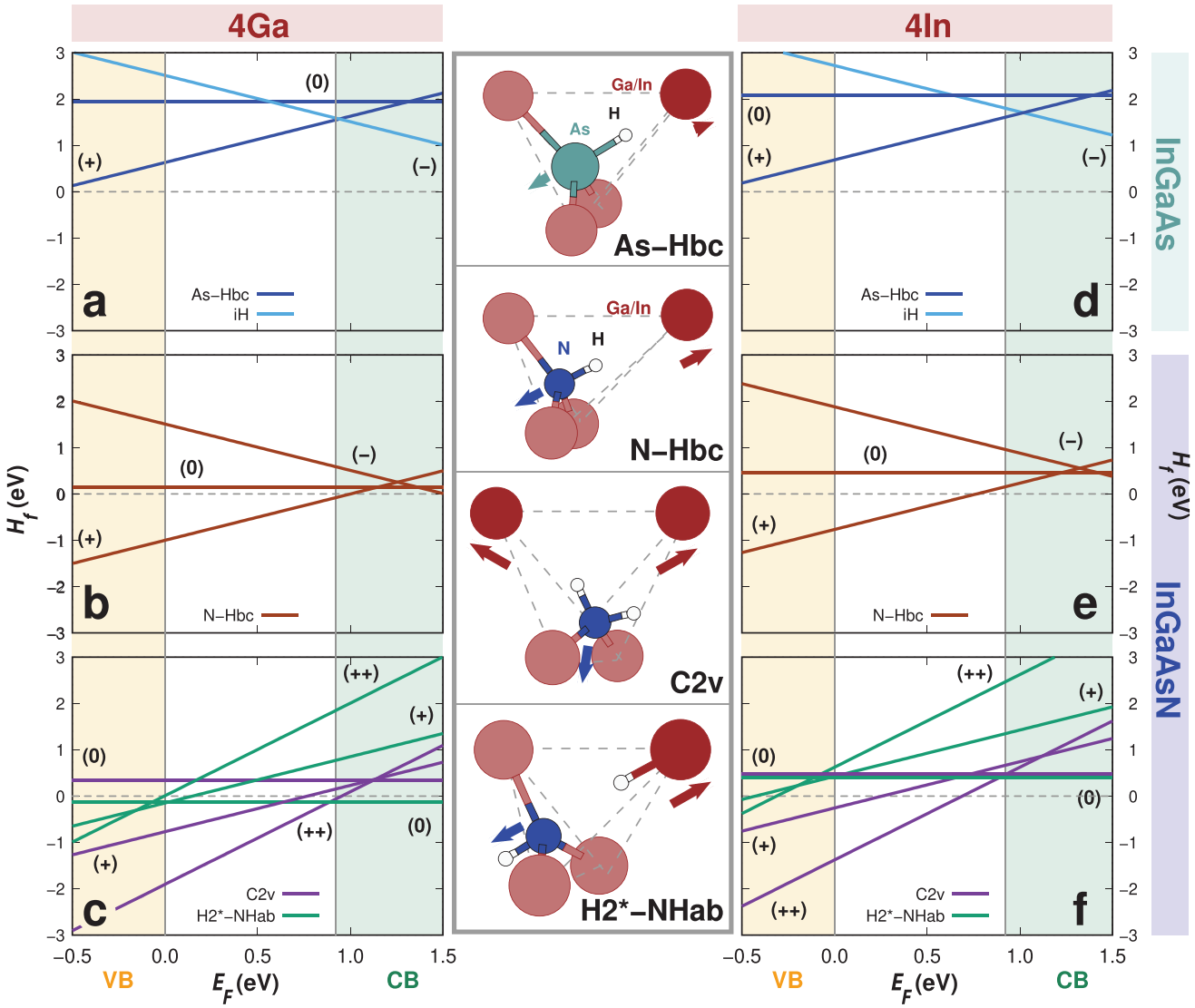

Figure 3. The geometries of the most important As-H and N–H complexes investigated here are shown in the central panel of the figure. The arrows highlight the displacements of the atoms in the complex from their unrelaxed position. The dashed lines draw a tetrahedron formed by the four Ga or In atoms neighboring the N atom involved in the complex. The three topmost sketches refer to bc and C_{2v} complexes, the bottom-most one to two H atoms located at a bc site and an ab (anti-bonding) site on the N side of the Ga(or In)-H_{bc}-N-H_{ab} complex (also referred to as H_2^*ab complex). a–f) Formation energies of different As-H and N–H complexes as a function of the Fermi level. The range of the energy gap, 0.0–0.92 eV, corresponds to the estimated, partially recovered InGaAs energy gap, see the Section 3.2.

Driven by previous studies on hydrogenated $GaAs_{1-x}N_x$,[1,4–6,19] $InAs_{1-x}N_x$,[15] and $In_yGa_{1-y}As_{1-x}N_x$,[20,21] as well as $In_{1-x}Ga_xN$ alloys,[22] we investigated several complexes coming from the interactions of H atoms with host and N atoms. Such investigations concerned geometries, formation energies H_f,[23] formation reactions and DFT Heyd–Scuseria–Ernzerhof hybrid functional (DFT-HSE)[24] energy gaps.

In the InGaAsN lattice, a H atom can form a charged As-H_{bc}(+) or a neutral As-H_{bc}(0) complex (see **Figure 3**), where H is located at the bc (bond-centered) site of a Ga-As (or In-As) bond that is broken and replaced by an As-H bond. Alternatively, H can form a iH(–1) complex (not shown in Figure 3) where a H atom occupies an almost tetrahedral interstitial site in the lattice. Figure 3a,d shows the H_f dependence on the Fermi level (E_F) of these three complexes, in the 4Ga-As and 4In-As environments, respectively. The H_f graphs show the stable charge state for each complex at different E_F values. The crossing point between two H_f lines defines the transition level value, $\varepsilon(n/n+1)$, that is, the E_F position where a complex changes its charge state from n to $n+1$.[19,23] The As-H_{bc}(+) H_f line does not cross the other ones in the whole energy gap range, that is, the complex is always stable in the +1 charge state. This indicates a shallow donor behavior of H.

H_{bc}(+) ions migrate in the crystal lattice attracted by the N negative charge,[1] giving rise to exothermic reactions like, for example, (4Ga)N + As-H_{bc}(+) → (4Ga)N–H_{bc}(+), see Section S2, Supporting Information. Given the shallow donor behavior of H, this reaction is the only possible initial step for the formation of an N–H complex in the InGaAsN lattice.

Table 2. The first row of the Table reports the DFT-HSE band gap energies, E_g (eV), calculated by using the 4Ga-N (as-grown alloy) and 4In-N (annealed alloy) InGaAsN models without hydrogen. E_g values induced by the formation of N–H_{bc}(+) and C_{2v}+2 N–H complexes with the corresponding 4Ga-N and 4In-N clusters are given in the second row. For a comparison, the calculated InGaAs energy gap is 1.01 eV.

	4Ga-N	4In-N	4Ga-N	4In-N
	H_{bc}(+)	H_{bc}(+)	C_{2v}+2	C_{2v}+2
E_g(InGaAsN) [eV]	0.66	0.81	0.66	0.81
E_g(InGaAsN + H) [eV]	0.86	0.93	1.04	1.03

The N–H_{bc}(+) complex could acquire one or two free electrons to form a neutral or negatively charged complex. At variance with As-H, no geometry rearrangement is found and N–H_{bc}(0) and N–H_{bc}(–) complexes result to be the most stable neutral and negatively charged complexes, respectively. Their H_f values are reported in Figure 3b,e, together with the N–H_{bc}(+) ones, for the 4Ga-N and 4In-N clusters, respectively. H behaves as a shallow donor in both N environments.

Di-hydrogen complexes were also investigated: the C_{2v} one,[1,25–27] see Figure 3, clearly identified in $GaAs_{1-x}N_x$,[1,26,28,29] and various H_2^*-like complexes having on-line configurations where two H atoms occupy a bc and/or an ab sites (see Figure 3 and Section S3, Supporting Information). Only the most stable H_2^* complex, that is, the H_2^* Ga(or In)-H_{bc}-N–H_{ab} complex (also referred to as H_2^*ab complex) is shown in Figure 3. H_2^* complexes were recently proposed in InGaAsN. [20,21]

In InGaAsN, given the predominance of H_{bc}(+) species, both C_{2v} and H_2^* complexes can initially form only in the +2 charge state and then possibly acquire free electrons and modify their geometries through H atom re-orientations. Therefore, we investigated the +2, +1, and 0 charge states of these complexes for both 4Ga-N and 4In-N clusters, see Section S3, Supporting Information. H_f values of the C_{2v} and H_2^*ab complexes are shown in Figure 3c,f for the two N environments, respectively. In both cases, the C_{2v} complexes are stable in the +2 charge state and lower in energy than the H_2^*ab+2 complex in the whole energy gap range. This rules out the formation of H_2^* complexes.

The H-induced neutralization of the effects of N was investigated by considering the DFT-HSE energy gaps calculated for the 4Ga-N (as-grown alloy) and 4In-N (annealed alloy) models without H and for the N–H_{bc}(+) and C_{2v}+2 complexes formed with the corresponding N clusters, see **Table 2**.

The energy gap of the 4In-N alloy model increases with respect to that of the 4Ga-N one, in agreement with the trend shown by the experimental gaps of the corresponding alloys (see Table 1). N–H_{bc}(+) complexes increase the energy gap but they do not fully recover the InGaAs gap, 1.01 eV, in the cases of both 4Ga-N and 4In-N clusters, while C_{2v}+2 complexes do, in both N environments. The homogeneous behavior of these two complexes in the two N environments gives an important indication: only different ratios between the concentrations of the two complexes in the as-grown and annealed InGaAsN could explain why H seems much more effective in neutralizing the effects of N in the as-grown material (predominantly Ga-rich N environment) than in the annealed samples (increasingly In-rich N environment).

Complex concentrations are controlled by kinetic effects related to the experimental hydrogenation conditions. Their accurate estimate is, therefore, beyond the scope of the present study. Nevertheless, important indications can be given by the formation energies of Figure 3, which permit to estimate the concentration of each complex in thermodynamic equilibrium conditions. In InGaAsN, H_f values must be taken with respect to the bottom of the conduction band (BCB), where the E_F level is pinned by the H shallow donor behavior, see **Figure 4**.

As shown in Figure 4, with respect to the BCB, the H_f values of the N–H_{bc}(+) and C_{2v}+2 complexes are nearly identical for the 4Ga-N cluster, whereas they are significantly different in the 4In-N environment. From these H_f values, the estimates of the ratios between the concentrations of the two complexes (at room temperature) [N–H_{bc}(+)]/[C_{2v}+2] are much different, equal to 4×10^3 and ≈7, in the cases of 4In-N clusters and 4Ga-N clusters, respectively (see Section 3.2).

Although the above estimates hold only at thermodynamic equilibrium (not reached in the present experiments), such a striking difference between the two ratios led us to assume a substantial coexistence of the two complexes in the Ga-rich N environment, replaced by a full predominance of the N–H_{bc}(+) complex in the In-rich one. These results, together with those reported in Table 2, already give a full, qualitative explanation of the experimental findings. In the as-grown InGaAsN alloy, the absence of a full energy gap recovery following H irradiation is indeed accounted for by the predominance of 4Ga-N clusters and by the ensuing coexistence of two complexes, among which only the C_{2v}+2 fully neutralizes the effects of N. In the annealed alloys, the increasing preponderance of 4In-N clusters hinders the formation of the complex most effective for N passivation, thus accounting for the observed reduction in hydrogen's ability to cause the energy gap recovery. The above estimates of the N–H_{bc}(+) and C_{2v}+2 concentrations can be used for a refinement of the results of Table 2, leading to a satisfactory agreement with the experiment, see Section S4, Supporting Information. Here, we focus on a puzzling question posed by the above results: why do N–H complexes showing such similar properties form in much different concentration ratios when the cation-N environment changes? Our answer implies a change of perspective. Let us consider the N–H_{bc}(+) and C_{2v}+2 complexes forming in InGaAsN, either in the 4Ga-N or in the 4In-N environment, as units inserted in the host InGaAs matrix. Then, let us compare their formation with that of the same units in the GaAsN and InAsN alloys, where they necessarily form in the 4Ga-N and 4In-N environments and are inserted in the GaAs and InAs matrices, respectively. What is the advantage of such a comparison? For the N–H_{bc}(+) complex in InGaAsN, the breaking of a Ga-N or an In-N bond and its replacement by a N–H bond induces an increase of the cation-N distance of more than a 60%, see Figure 3. This implies a significant local strain around the N atom, which gets even higher in the case of the C_{2v}+2 complex, where the number of bonds broken and replaced amounts to 2.[30] The energy balance governing the formation of either complex consists of two contributions: the balance of chemical bond energies and the cost in energy due to the local strain. When investigating a given complex, for example, the C_{2v}+2 in the 4In-N (4Ga-N) environment, the bond energy balance is almost identical in InGaAsN and InAsN (GaAsN), as it corresponds to the dissociation and formation of almost identical chemical bonds (see Section S2, Supporting Information). Therefore, most of the difference in the energetics of the complexes may be ascribed to the difference in the strain energy.

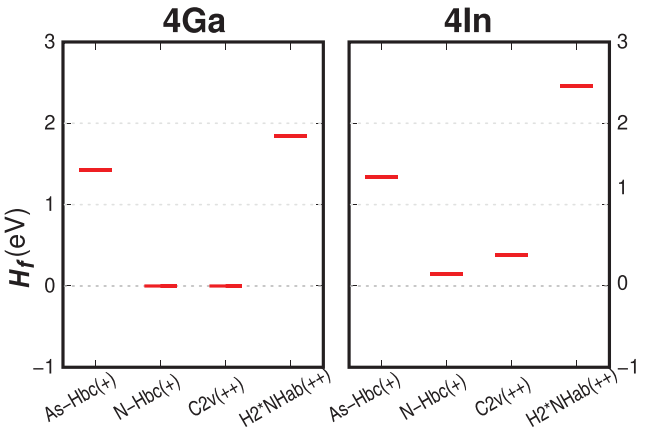

Figure 4. . Formation energies H_f of the most important As-H and N–H charged complexes, taken from Figure 3 with respect to the bottom of the conduction band (BCB), are reported as red lines in the figure.

In InGaAsN and InAsN (GaAsN) alloys, the local strain induced by the formation of a N–H complex in the 4In-N (4Ga-N) environment can be related to the volume expansion of the 4In (4Ga) tetrahedron surrounding the N atom, see Figure 3. In fact, for example, in InAsN, the volumes of the N–H_{bc}(+) and C_{2v}+2 N-tetrahedra increase by 55% and 126% with respect to that of an isolated N atom, respectively. In InGaAsN, the corresponding volume expansions amount to 47% and 102%, respectively. The two complexes show smaller volume expansions in InGaAsN because the N-tetrahedron expands against a host InGaAs matrix which has a smaller unit cell and a larger bulk modulus (i.e., a larger stiffness) than the host InAs matrix of InAsN (see Section S5, Supporting Information). Thus, both the N–H_{bc}(+) and the C_{2v}+2 complexes have to pay a higher strain energy cost when forming in the stiffer host matrix, as testified by the decrease of the corresponding tetrahedron volume expansions. Of course, the formation of the C_{2v}+2 complex, which requires a larger tetrahedron expansion than N–H_{bc}(+), is more severely affected by the stiffness of the host matrix. This critical, discriminating effect on the formation of the two complexes can be quantified by estimating the ratios between the volume expansions of the C_{2v}+2 and N–H_{bc}(+) tetrahedra in InGaAsN and InAsN, 2.17 and 2.29, respectively. These values confirm the larger hindrance influencing the C_{2v}+2 formation (with respect to N–H_{bc}(+)) in InGaAsN. Albeit small, their difference is a significant one. In fact, let us consider the 4Ga-N environment and examine the formation of the same two complexes in InGaAsN and in GaAsN. Now, the InGaAs matrix is the one with a larger unit cell and a smaller bulk modulus with respect to GaAs (see Section S5, Supporting Information); therefore, there is a lower opposition to the formation of these complexes in InGaAsN than in GaAsN. In the two materials, indeed, the volumes of the C_{2v}+2 N-tetrahedron increase by 129% and 124%, while those of the N–H_{bc}(+) N-tetrahedron are 55% and 53% higher, respectively. At variance with the previous case, the larger increase occurs now in InGaAsN. Moreover, the ratio between the volume expansions of the two complexes is equal to 2.34 in both alloys, showing that the different opposition to their formation, found in the InGaAsN-InAsN comparison, has disappeared. Accordingly, when in a 4Ga-N environment in InGaAsN, the C^{2v} +2 and the N–H_{bc}(+) complexes form in comparable concentrations, as suggested by the H_f values in Figure 4.

The above considerations (further results in Section S5, Supporting Information) lead to the remarkable conclusion that for N–H complexes forming in the 4In-N environment, and only in this environment, the InGaAsN host matrix exerts a selective action favoring the formation of the N–H_{bc}(+) complex (less effective in neutralizing the effects of N), thus explaining thoroughly the occurrence of different N–H complex concentrations in the two different cation-N environments. This result also fully accounts for the experimental observation that annealed InGaAsN samples (predominant In-rich N environment) are significantly less sensitive to H irradiation than the nonannealed material (predominant Ga-rich environment).

The present results reveal, therefore, the existence of a novel physical phenomenon, where a major role is played by the matrix surrounding the N–H complex. They also clarify its origin, which is traced back to the two-component nature of the InGaAs alloy, more specifically, to the different mechanical properties of its GaAs and InAs components. This important finding could open further routes for the development of new protocols for the tuning of the material properties, which can be based on an integrated matrix/defect engineering approach, with immediate impact on both the material design and the realization of quantum confining structures. About the former feature, the proposed model is not limited to III–V-N alloys, under the (very reasonable) assumption that it may be generalized to alloys presenting parallel features, for example, N doped SiC, SiC:N, where C:N and Si:N play the role of GaAsN and InAsN, respectively.[31–33] Regarding the quantum structures, for example, as-grown InGaAsN could be locally annealed by exposure to a focused laser beam. Upon hydrogenation these annealed regions would be lower-energy gap areas, wherein carriers could be laterally confined. In principle, the size of these carrier-confining potentials could be pushed to the nanoscale by applying the subwavelength light-focusing techniques recently applied to the fabrication of site-controlled GaAsN:H/GaAsN quantum dots,[10,11] thus demonstrating the potential of the novel approach proposed here.

3. Experimental Section

Experimental Details: Two types of $In_yGa_{1-y}As_{1-x}N_x$/GaAs QW samples grown by metalorganic vapor phase epitaxy on a GaAs substrate were investigated. The first type consisted in a double QW structure,[34] with the $In_yGa_{1-y}As_{1-x}N_x$ QW on top of the $In_yGa_{1-y}As$ QW. The deposition sequence is as follows. First, a thick (200 nm) GaAs buffer was grown at 590 °C. After a growth interruption to decrease the temperature down to 520 °C, the 5.6 nm-thick $In_{0.25}Ga_{0.75}As$ reference QW was deposited and the temperature was brought back to 590 °C. During this process the arsine flux was kept high (As/III = 100). A 50 nm GaAs layer was then deposited before interrupting again the growth to lower the reactor temperature. The $In_{0.25}Ga_{0.75}As_{1-x}N_x$ QW (thickness equal to 5.6 nm as the reference QW) was deposited using a 2-step growth method intended to prevent the N accumulation at the first growth interface. The InGaAsN was deposited in two successive layers: 1.5 nm at 520 °C with moderate DMHy flux (26 ccm) followed by 4.1 nm with higher flux (190 ccm). The As/III = 8 ratio was kept low during the N-containing QW

deposition, and a similar arsine flux was used during the last minutes of the preceding growth interruption. The N concentration was estimated by PL to be ≈0.015. The temperature was finally increased to 590 °C to deposit a 100 nm GaAs cap.

The second type of sample consisted in a single $In_yGa_{1-y}As_{1-x}N_x$/GaAs QW. The deposition sequence is as follows. First, a thick (250 nm) GaAs buffer was grown at 650 °C. After a growth interruption to decrease the temperature down to 525 °C, a 5 nm thick $In_{0.21}Ga_{0.79}As_{0.97}N_{0.03}$ QW was deposited. The As/Ga ratio was kept at 7 during the QW growth. The UDMHy/TBAs ratio for the QW growth was 67. After the QW growth, a 90 nm thick GaAs cap was grown also at 525 °C. Subsequently the sample was annealed for 5 min at 725 °C under TBAs stabilization. The sample was also annealed ex situ in an N_2 environment under atmospheric pressure with a GaAs proximity cap. The heating ramp was in the range of 7 K s^{-1}. Three annealing conditions were employed: 600 °C for 10 s, 650 °C for 30 s, and 750 °C for 10 s. As reported previously,[16] these conditions modified the atomic rearrangement in the InGaAsN lattice without changing the average composition of the QW (namely, without causing In/Ga diffusion in the barrier/QW).

Finally, the samples were proton- or deuteron-irradiated at $T_I = 300$ °C by a Kaufman source (100 eV per ion beam energy) with typical ion impinging current density of few tens of μA cm^{-2}.

PL measurements were recorded at room temperature, in order to avoid contribution from the localized states that typically dominate the spectra at cryogenic temperatures ($T < 150$ K).[35] This allowed to reliably determine the effective band gap energy of the QW, which was assumed to coincide with the PL peak energy. PL was excited by a 532 nm laser, spectrally analyzed by a 0.75 m focal length monochromator and detected by a liquid nitrogen-cooled InGaAs linear array.

SIMS measurements were performed on the double QW sample treated with deuterium (D is equivalent to H in terms of its interaction with N, but SIMS measurements are experimentally more sensitive to the heavier isotope). A E_{Cs}=1 keV Cs^+ primary beam at oblique incidence (55°) was used in a CAMECA Sc-Ultra mass spectrometer where $^2D^-$, $^{14}N^-$, $^{70}Ga^-$, and $^{115}In^-$ negative secondary ions were collected with a depth resolution of 2–3 nm $decade^{-1}$. Other impact energies and incidence angles versus surface normal were tested in order to identify the best analytical conditions for this class of samples. 1 keV at 55° were the best conditions for signal to noise ratio and for depth resolution. The sputtering time was converted to an in-depth scale by measuring the obtained crater depths by a mechanical stylus profilometer.

Theoretical Methods: DFT-HSE with the range-separated HSE06 hybrid functional,[24,36] as implemented with plane wave basis sets in the QUANTUM-ESPRESSO[37,38] suite of programs was used here for the investigation of the equilibrium structures and electronic properties of the InGaAsN alloy and of the complexes formed by atomic H with N and with the host atoms in this alloy, as well as for understanding the effects of the complex formation on the host energy gap. In this regard, as performed in a previous study,[15] in all of the systems investigated here the energy gap values were estimated by the Kohn–Sham (KS) hybrid functional eigenvalues. The properties of hydrogenated and pristine InGaAsN and InGaAs alloys were investigated by using 64-atom supercells simulating $In_{0.20}Ga_{0.80}As_{0.97}N_{0.03}$ and $In_{0.20}Ga_{0.80}As$ alloys close in stoichiometry to the measured samples, where the Ga and In cations were randomly distributed (see Section S1, Supporting Information). 64-atom supercells assured a satisfactory convergence in the case of GaAs and GaAsN.[15] Thus, they were used here for the investigation of the present GaAs-rich alloys. Nuclei and core electrons were substituted by optimized norm-conserving Vanderbilt's pseudopotentials.[39] Explicit valence pseudo-wavefunctions were 2s and 2p for N; 3s and 3p for As; 3d, 4s and 4p for Ga; 4d, 5s and 5p for In. The plane wave and density cutoffs were 80 and 320 Ry, respectively. The short-range part of the hybrid exchange functional is defined as a linear combination of exact Hartree–Fock exchange and GGA exchange

$$E_x^{hybr} = \alpha E_x^{Fock} + (1-\alpha)E_x^{GGA} \quad (1)$$

In a previous study of N–H complexes in the GaAsN and InAsN alloys,[15] the coefficient α was chosen in order to best describe the KS band gap of InAs, given the rather small energy gap of this semiconductor: α = 0.32 was the best choice. Errors induced in the InAs and GaAs KS band gaps were around 0.2% and 7%, respectively. Errors on the InAsN and GaAsN energy gaps amounted to 16% and 17%, respectively. In order to perform a consistent comparison between previous and present results, the same value for the α parameter was used here. This led to errors of 29% and 20%, with respect to the experimental data, when the as-grown and annealed InGaAsN alloys were simulated by $In_{0.20}Ga_{0.80}As_{0.97}N_{0.03}$ models containing only 4Ga-N and 4In-N clusters, respectively. Notwithstanding, present results gave reliable indications on the H effects on the energy gap. In fact, first, the calculated $In_{0.20}Ga_{0.80}As$ energy gap, 1.01 eV, was affected by a comparable error of about 23% with respect to the estimated value of 1.32 eV corresponding to the vertical dashed line labeled as ref. in Figure 2b of the main text. Second, N–H complexes raising the energy gap to its theoretical value (1.01 eV) guaranteed a full passivation of the N effects.

Given the heavy computational demand of hybrid functional simulations, geometry optimizations were performed sampling the Brillouin zone at the Γ point. Total energies and electronic eigenvalues were obtained by single-point calculations on a $2 \times 2 \times 2$ **k**-point mesh including the Γ point.

In the present study, a further fundamental quantity was the formation energy of a complex formed by H with the N atom and/or the host atoms, H_f. For instance, in the case of a N–H complex in the q charge state and containing n H atoms, H_f is given by the expression (see, e.g., Ref. [23, 40], and references therein)

$$H_f[N-nH](q) = E[N-nH](q) - E[N] - n\mu_H + q(E_F + \varepsilon_{VB}) \quad (2)$$

where $E[N-nH](q)$ and $E[N]$ are the total energies of the supercells containing the complex in a charge state q, and, respectively, the nitride alloy without H. The third term keeps into account the addition to the system of n hydrogen atoms ($n > 0$), considered at a chemical potential μ_H. Here, μ_H corresponds to half of the total energy of a H_2 molecule in vacuum. Electrons were given to or taken from (in agreement with the q value) a reservoir, whose chemical potential was the Fermi level E_F, referred to the valence band maximum, ϵ_{VB}. Thus, it is seen from Equation (2) that the formation energies H_f follow the Fermi level E_F as straight lines, whose slope is given by the complex charge, q, as shown in Figure 3.

Formation energies as defined in Equation (2) may be used to determine the charge states of a complex in the system as a function of the Fermi level of the electron reservoir. Equating formation energies of the N-nH complex in the charge states q and q' gives the transition level

$$\varepsilon(q/q') = \frac{E[N-nH](q') - E[N-nH](q)}{q-q'} - \varepsilon_{VB} \quad (3)$$

that is the Fermi level value at which the complex passes from charge q to charge q'.[23]

The formation energy of a N–H complex had to be computed for values of E_F within a given energy gap range. When H fully passivates the effects of N (e.g., in the case of GaAsN), the energy gap range was that of the material without N (i.e., GaAs). In InGaAsN, it had to be taken into account that H recovered only a 91% of the InGaAs gap, as shown by the experimental data reported in Figure 1, where 1.115 and 1.220 eV energy gaps were measured for the hydrogenated InGaAsN QW and for the pristine InGaAs QW, respectively. According to the simulations, the theoretical estimate of the InGaAs gap is equal to 1.01 eV. Thus, the maximum value reachable by the energy gap of the hydrogenated InGaAsN is equal to 0.92 eV, as reported in Figures 3 and 4.

Formation energies also permitted to estimate the concentration of an X complex in thermodynamic equilibrium conditions, [X], which is given by the expression[23]

$$[X] = N_{sites} N_{config} \exp(-H_f^X / kT), \quad (4)$$

where N_{sites} is the number of sites in the lattice per unit volume where the complex can be incorporated, N_{config} is the number of equivalent configurations in which the complex can be formed, k is the Boltzmann's constant, and T is the temperature.

Here, the need is to estimate the ratio of the complex concentrations, $[N–H_{bc}(+)]/[C_{2v}+2]$ or $[X1]/[X2]$, that is:

$$[X1]/[X2] = R_{config} \exp\left[\left(H_f^{X2} - H_f^{X1}\right)/kT\right] \quad (5)$$

where it has been taken into account that N_{sites} has the same value for both complexes and the ratio $N_{config}(X1)/N_{config}(X2)$, R_{config}, is equal to 0.67.

Supporting Information

Supporting Information is available from the Wiley Online Library or from the author.

Acknowledgements

The authors would like to acknowledge Dr. Alok Rudra, from Ecole Polytechnique Fédérale de Lausanne (EPFL), Switzerland, for his precious support to the logistics of the MOVPE facility in the Laboratory of Physics of Nanostructures.

Open access funding provided by Consiglio Nazionale delle Ricerche within the CRUI-CARE Agreement.

Conflict of Interest

The authors declare no conflict of interest.

Data Availability Statement

Research data are not shared.

Keywords

density functional theory, hydrogen doping, InGaAsN alloys

Received: September 6, 2021
Revised: October 4, 2021
Published online: October 22, 2021

[1] *Hydrogenated Dilute Nitride Semiconductors* (Ed: G. Ciatto), Pan Stanford, Singapore **2015**.
[2] A. Albo, D. Fekete, G. Bahir, *Infrared Phys. Technol.* **2019**, *96*, 68.
[3] M. Felici, A. Polimeni, G. Salviati, L. Lazzarini, N. Armani, F. Masia, M. Capizzi, F. Martelli, M. Lazzarino, G. Bais, M. Piccin, S. Rubini, A. Franciosi, *Adv. Mater.* **2006**, *18*, 1993.
[4] Y.-S. Kim, K. J. Chang, *Phys. Rev. B* **2002**, *66*, 073313.
[5] A. Janotti, S. B. Zhang, S.-H. Wei, C. G. Van de Walle, *Phys. Rev. Lett.* **2002**, *89*, 086403.
[6] A. Amore Bonapasta, F. Filippone, P. Giannozzi, M. Capizzi, A. Polimeni, *Phys. Rev. Lett.* **2002**, *89*, 216401.
[7] E. P. O'Reilly, A. Lindsay, P. J. Klar, A. Polimeni, M. Capizzi, *Semicond. Sci. Technol.* **2009**, *24*, 033001.
[8] P. J. Klar, H. Grüning, M. Güngerich, W. Heimbrodt, J. Koch, T. Torunski, W. Stolz, A. Polimeni, M. Capizzi, *Phys. Rev. B* **2003**, *67*, 121206(R).
[9] M. Felici, G. Pettinari, F. Biccari, A. Boschetti, S. Younis, S. Birindelli, M. Gurioli, A. Vinattieri, A. Gerardino, L. Businaro, M. Hopkinson, S. Rubini, M. Capizzi, A. Polimeni, *Phys. Rev. B* **2020**, *101*, 205403.
[10] F. Biccari, A. Boschetti, G. Pettinari, F. La China, M. Gurioli, F. Intonti, A. Vinattieri, M. Sharma, M. Capizzi, A. Gerardino, L. Businaro, M. Hopkinson, A. Polimeni, M. Felici, *Adv. Mater.* **2018**, *30*, 1705450.
[11] A. Ristori, T. Hamilton, D. Toliopoulos, M. Felici, G. Pettinari, S. Sanguinetti, M. Gurioli, H. Mohseni, F. Biccari, *Adv. Quantum Technol.* **2021**, *4*, 2100045.
[12] Y. Park, M. J. Cich, R. Zhao, P. Specht, H. Feick, E. R. Weber, *Phys. B: Condens. Matter* **2001**, *308–310*, 98.
[13] S. Birindelli, M. Kesaria, D. Giubertoni, G. Pettinari, A. V. Velichko, Q. D. Zhuang, A. Krier, A. Patanè, A. Polimeni, M. Capizzi, *Semicond. Sci. Technol.* **2015**, *30*, 105030.
[14] A. V. Velichko, A. Patanè, M. Capizzi, I. C. Sandall, D. Giubertoni, O. Makarovsky, A. Polimeni, A. Krier, Q. Zhuang, C. H. Tan, *Appl. Phys. Lett.* **2015**, *106*, 022111.
[15] F. Filippone, G. Mattioli, A. Polimeni, M. Felici, A. Amore Bonapasta, *J. Phys. Chem. C* **2020**, *124*, 19240.
[16] C. Peng, H. Liu, J. Konttinen, M. Pessa, *J. Cryst. Growth* **2005**, *278*, 259.
[17] P. J. Klar, H. Grüning, J. Koch, S. Schäfer, K. Volz, W. Stolz, W. Heimbrodt, A. M. K. Saadi, A. Lindsay, E. P. O'Reilly, *Phys. Rev. B* **2001**, *64*, 121203.
[18] S. Kurtz, J. Webb, L. Gedvilas, D. Friedman, J. Geisz, J. Olson, R. King, D. Joslin, N. Karam, *Appl. Phys. Lett.* **2001**, *78*, 748.
[19] C. Van de Walle, J. Neugebauer, *Nature* **2003**, *423*, 626.
[20] T. Mou, S. Li, C. R. Brown, V. R. Whiteside, K. Hossain, M. Al Khalfioui, M. Leroux, I. R. Sellers, B. Wang, *ACS Appl. Electron. Mater.* **2019**, *1*, 461.
[21] C. R. Brown, N. J. Estes, V. R. Whiteside, B. Wang, K. Hossain, T. D. Golding, M. Leroux, M. Al Khalfioui, J. G. Tischler, C. T. Ellis, E. R. Glaser, I. R. Sellers, *RSC Adv.* **2017**, *7*, 25353.
[22] G. Pettinari, F. Filippone, A. Polimeni, G. Mattioli, A. Patané, V. Lebedev, M. Capizzi, A. Amore Bonapasta, *Adv. Funct. Mater.* **2015**, *25*, 5353.
[23] C. G. Van de Walle, J. Neugebauer, *J. Appl. Phys.* **2004**, *95*, 3851.
[24] J. Heyd, G. E. Scuseria, M. Ernzerhof, *J. Chem. Phys.* **2006**, *124*, 219906.
[25] A. Amore Bonapasta, F. Filippone, P. Giannozzi, *Phys. Rev. B* **2003**, *68*, 115202.
[26] W. B. Fowler, K. R. Martin, K. Washer, M. Stavola, *Phys. Rev. B* **2005**, *72*, 035208.
[27] M.-H. Du, S. Limpijumnong, S. B. Zhang, *Phys. Rev. B* **2005**, *72*, 073202.
[28] S. Kleekajai, F. Jiang, K. Colon, M. Stavola, W. B. Fowler, K. R. Martin, A. Polimeni, M. Capizzi, Y. G. Hong, H. P. Xin, C. W. Tu, G. Bais, S. Rubini, F. Martelli, *Phys. Rev. B* **2008**, *77*, 085213.
[29] L. Wen, F. Bekisli, M. Stavola, W. B. Fowler, R. Trotta, A. Polimeni, M. Capizzi, S. Rubini, F. Martelli, *Phys. Rev. B* **2010**, *81*, 233201.
[30] A. Polimeni, G. Ciatto, L. Ortega, F. Jiang, F. Boscherini, F. Filippone, A. Amore Bonapasta, M. Stavola, M. Capizzi, *Phys. Rev. B* **2003**, *68*, 085204.
[31] M. N. R. Ashfold, J. P. Goss, B. L. Green, P. W. May, M. E. Newton, C. V. Peaker, *Chem. Rev.* **2020**, *120*, 5745.
[32] F. Casola, T. van der Sar, A. Yacoby, *Nat. Rev. Mater.* **2018**, *3*, 17088.
[33] J. Y. Tsao, S. Chowdhury, M. A. Hollis, D. Jena, N. M. Johnson, K. A. Jones, R. J. Kaplar, S. Rajan, C. G. Van de Walle, E. Bellotti, C. L. Chua, R. Collazo, M. E. Coltrin, J. A. Cooper, K. R. Evans,

S. Graham, T. A. Grotjohn, E. R. Heller, M. Higashiwaki, M. S. Islam, P. W. Juodawlkis, M. A. Khan, A. D. Koehler, J. H. Leach, U. K. Mishra, R. J. Nemanich, R. C. N. Pilawa-Podgurski, J. B. Shealy, Z. Sitar, M. J. Tadjer, et al., *Adv. Electron. Mater.* **2018**, *4*, 1600501.

[34] D. Fekete, R. Carron, P. Gallo, B. Dwir, A. Rudra, E. Kapon, *Appl. Phys. Lett.* **2011**, *99*, 072116.

[35] A. Polimeni, M. Capizzi, M. Geddo, M. Fischer, M. Reinhardt, A. Forchel, *Appl. Phys. Lett.* **2000**, *77*, 2870.

[36] J. Heyd, G. E. Scuseria, M. Ernzerhof, *J. Chem. Phys.* **2003**, *118*, 8207.

[37] P. Giannozzi, O. Andreussi, T. Brumme, O. Bunau, M. B. Nardelli, M. Calandra, R. Car, C. Cavazzoni, D. Ceresoli, M. Cococcioni, N. Colonna, I. Carnimeo, A. D. Corso, S. de Gironcoli, P. Delugas, R. A. DiStasio, A. Ferretti, A. Floris, G. Fratesi, G. Fugallo, R. Gebauer, U. Gerstmann, F. Giustino, T. Gorni, J. Jia, M. Kawamura, H.-Y. Ko, A. Kokalj, E. Küçükbenli, M. Lazzeri, et al., *J. Phys.: Condens. Matter* **2017**, *29*, 465901.

[38] P. Giannozzi, S. Baroni, N. Bonini, M. Calandra, R. Car, C. Cavazzoni, D. Ceresoli, G. L. Chiarotti, M. Cococcioni, I. Dabo, A. D. Corso, S. de Gironcoli, S. Fabris, G. Fratesi, R. Gebauer, U. Gerstmann, C. Gougoussis, A. Kokalj, M. Lazzeri, L. Martin-Samos, N. Marzari, F. Mauri, R. Mazzarello, S. Paolini, A. Pasquarello, L. Paulatto, C. Sbraccia, S. Scandolo, G. Sclauzero, A. P. Seitsonen, et al., *J. Phys.: Condens. Matter* **2009**, *21*, 395502.

[39] D. R. Hamann, *Phys. Rev. B* **2013**, *88*, 085117.

[40] W. Chen, A. Pasquarello, *J. Phys.: Condens. Matter* **2015**, *27*, 133202.

ADVANCED FUNCTIONAL MATERIALS

Supporting Information

for *Adv. Funct. Mater.,* DOI: 10.1002/adfm.202108862

Selective Effects of the Host Matrix in Hydrogenated InGaAsN Alloys: Toward an Integrated Matrix/Defect Engineering Paradigm

Francesco Filippone, Saeed Younis, Giuseppe Mattioli, Marco Felici, Elena Blundo, Antonio Polimeni, Giorgio Pettinari, Damiano Giubertoni, Eduard Sterzer, Kerstin Volz, Dan Fekete, Eli Kapon, and Aldo Amore Bonapasta*

Selective effects of the host matrix in hydrogenated InGaAsN alloys: towards an integrated matrix/defect engineering paradigm. Supplementary Information.

Francesco Filippone,[1,*] Saeed Younis,[2] Giuseppe Mattioli,[1] Marco Felici,[2] Elena Blundo,[2] Antonio Polimeni,[2] Giorgio Pettinari,[3] Damiano Giubertoni,[4] Eduard Sterzer,[5] Kerstin Volz,[5] Dan Fekete,[6,7] Eli Kapon,[7] and Aldo Amore Bonapasta[1]

[1] *ISM-CNR, Istituto di Struttura della Materia – Consiglio Nazionale delle Ricerche, Via Salaria Km 29.5, I-00015 Monterotondo, Italy*

[2] *Dipartimento di Fisica and CNISM, Sapienza Università di Roma, Piazzale A. Moro 2, I-00185 Roma, Italy*

[3] *Istituto di Fotonica e Nanotecnologie (IFN) del Consiglio Nazionale delle Ricerche, via Cineto Romano 42, 00156 Roma, Italy*

[4] *Fondazione Bruno Kessler, Centre for Materials and Microsystems, Micro Nano Facility, Via Sommarive 18, 38123 Trento, Italy*

[5] *Department of Physics and Material Sciences Center, Philipps University Marburg, 35032 Marburg, Germany*

[6] *Department of Physics, Technion-Israel Institute of Technology, Haifa 32000, Israel*

[7] *Ecole Polytechnique Fédérale de Lausanne (EPFL), Laboratory of Physics of Nanostructures, CH-1015 Lausanne, Switzerland*

(Dated: July 14, 2021)

I. MODELING OF N ENVIRONMENTS AND INGAASN ALLOYS

In InGaAsN alloys, all the possible cation-N clusters ranging from 4Ga-N clusters to 4In-N clusters - $(4-n)$Ga(n)In-N clusters (n=0-4) - may ideally form. However, the many, possible configurations of single- and di-hydrogen N-H complexes in different charge states cannot be investigated by considering all of the above mentioned N clusters when using the highly computer-demanding DFT-HSE methods.

In the $In_{0.21}Ga_{0.79}As_{0.97}N_{0.03}$ model alloy here investigated, in a purely statistic approach, the 4Ga-N and 3Ga1In-N clusters should form about the 80% of the N clusters together with a remaining 20% including 2Ga2In-N, 1Ga3In-N, and 4In-N clusters. Thus, we introduced a first simplifying approximation regarding the N *environment* by assuming the 4Ga-N and 4In-N clusters as representatives of Ga-rich and In-rich N environments, respectively, and disregarding clusters of intermediate composition. These two clusters were used to investigate the properties of the N-H complexes. Then, we could show, a posteriori, that the main results achieved within this assumption can be extended to the intermediate clusters, thanks to the fact that the N-H complexes show fully homogeneous properties when involving a 4Ga-N or a 4In-N cluster. More specifically, each complex shows very similar structures, same relative stability, and same electronic charge in the two N environments. Thus, very reasonably, they exhibit the same properties in the case of the intermediate clusters.

A second approximation concerns the models used for the simulation of the as-grown and the annealed InGaAsN alloys. The experiments indicate that the as-grown alloy is characterized by a predominance of the Ga-rich N environment, the annealed alloy by a significant presence of the In-rich one. By including one N atom in a 64-atom supercell, we get an N 3% concentration, close to that of the investigated samples (2.5%). Thus, as an example, an attempt to include a number of Ga-rich and In-rich N clusters corresponding to the ratio expected in the as-grown alloy, 4:1, would require at least 5 N atoms in the supercell, that is, a 320-atom supercell, in order to maintain an N concentration of 3%. Clearly, this is an impossible task. Moreover, such an accuracy would be frustrated by the absence of any indication, from the experiment, of the ratio between Ga-rich and In-rich environments reached in the annealed alloys. Thus, we considered two "extreme" alloy models, characterized by the presence of 4Ga-N clusters only (actually, one cluster in the simulation supercells) and by that of 4In-N clusters only, for the investigation of the as-grown and the thermally annealed alloy, respectively. Once more, a posteriori, we could show that such an approximation gives reliable, albeit qualitative, indications about the most relevant issue object of the present investigation, that is, the ability of a given N-H complex to fully or partially neutralize the effects of N and recover the InGaAs energy gap. In fact, such an ability is homogeneously shown by each complex when it forms in a 4Ga-N or in a 4In-N cluster. For instance, the N-$H_{bc}(+)$ complex does not recover the InGaAs energy gap when it forms in either cluster. Thus, it would not recover the InGaAs energy gap even when inserted in a simulation supercell containing both N clusters.

All of the present theoretical calculations were performed within the two above approximations, by using 64-atom supercells where a 4Ga-N or a 4In-N cluster is embedded in an InGaAs matrix characterized by a random distribution of the Ga and In cations. In a preliminary step, in order to test the energetics of the alloy with respect to the number of In atoms first neighboring the N atom, we generated several random cation arrangements in a 64-atom supercell representing the $In_{0.22}Ga_{0.78}As_{0.97}N_{0.03}$ alloy (actually 7 In atoms on 32 positions), close in stoichiometry to the investigated

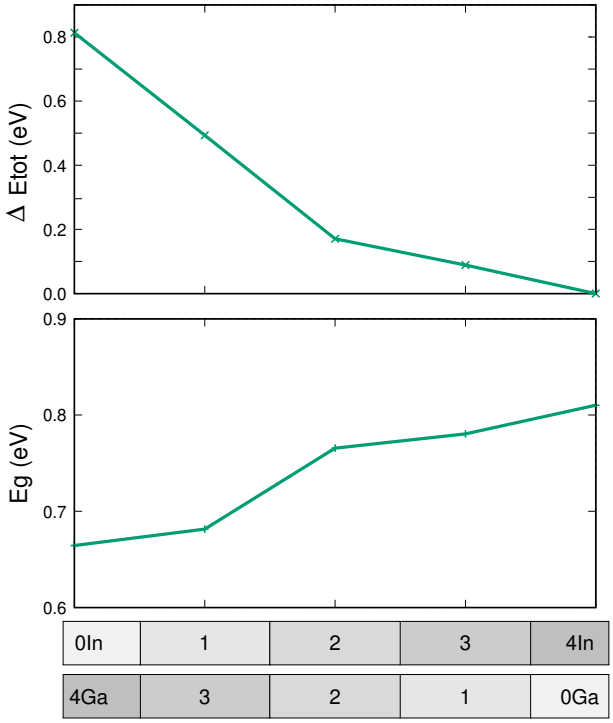

Figure 1. Trend of the total energy and the energy gap (Eg) calculated for the supercells simulating the $In_{0.22}Ga_{0.78}As_{0.97}N_{0.03}$ alloy and containing one cation-N cluster (with composition ranging from 4Ga-N to 4In-N) with respect to the number of In and Ga neighboring the N atom. Total energies (ΔEtot) are referred to the total energy of the supercell containing a 4In-N cluster.

$In_{0.21}Ga_{0.79}As_{0.975}N_{0.025}$ alloy samples. Then, we picked up the most stable arrangement and reorganized it for having 2, 3 or 4 In neighbors of the N atom. The total energies and the energy gaps calculated for supercells designed with the above procedure and containing different cation-N clusters are reported in Fig. 1. These results confirm an energetic gain of the alloy structure in clustering In cations around N, as shown by the decrease of the supercell total energy in the upper panel of the figure. On the contrary, the energy gap grows monotonically in increasing the number of In neighbors. Both the energetic gain and the parallel increase of the energy gap induced by the In clustering agree with the results of previous studies.[1–3] These studies showed also the increase of In-rich N environments in InGaAsN samples upon thermal annealing treatments. The supercells selected using the above procedure were used for the investigation of InGaAsN alloys without hydrogen as well as for that of the N-H complex properties.

The models described above gave first, qualitative results on the effects produced by a given complex on the alloy band gap, subsequently refined for an easier comparison with the experimental findings, as explained in a following section.

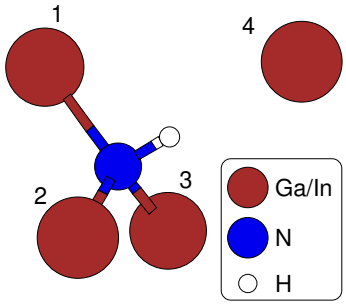

Figure 2. Schematic geometry of the N-H_{bc}(+) complex .

Table I. Atomic distances, d(X-Y), between the X and Y atoms involved in the N-H_{bc}(+) complex, whose geometry is schematized in Fig. 2. In the Table, the numbers in parentheses identify the cations neighboring the N atom, as indicated in Fig. 2. The labels of the columns indicate in which alloy or N environment the complex is formed, e.g., GaAsN or the 4Ga N environment in InGaAsN. All distances are given in Å.

	GaAsN	4Ga	4In	InAsN
d(N-(1))	2.05	2.07	2.20	2.24
d(N-(2))	2.05	2.05	2.21	2.24
d(N-(3))	2.05	2.06	2.20	2.24
d(N-(4))	3.55	3.61	3.53	3.78
d(N-H)	1.01	1.02	1.01	1.02
d(H-(4))	2.53	2.59	2.52	2.77

II. GEOMETRIES AND FORMATION REACTIONS OF SOME AS-H AND N-H COMPLEXES.

In the main text, it is stated that the formation of a N-H_{bc}(+) or a C_{2v}+2 complex in the 4In-N (4Ga-N) environment, is accompanied by a bond energy balance almost identical in InGaAsN and InAsN (GaAsN), as it corresponds to the dissociation and formation of almost identical chemical bonds. These statements are supported by the values of the bond distances given in Tables I and II for the N-H_{bc}(+) and C_{2v}+2 geometries shown in Figs. 2 and 3, respectively. In fact, regarding the bonds which are formed in the two N-H complexes, the results reported in the two Tables show that both complexes are characterized by the formation of very similar N-H and H-CT bonds (CT stands for a Ga or an In cation), when they form in the 4In-N (4Ga-N) environment in InGaAsN and in InAsN (GaAsN). In particular, the H atoms form strong N-H bonds and scarcely interact with the cations of the broken cation-N bonds. In Table II, the results reported for the not hydrogenated (pristine) alloys show that the Ga-N distances are almost identical in the cases of GaAsN and InGaAsN 4Ga-N environment, that is, quite similar bonds are broken when the N-H complexes form in either alloys. The same holds for the InAsN and the InGaAsN 4In-N environment.

The formation reactions of the investigated N-H complexes, mentioned in the main text, are schematized in

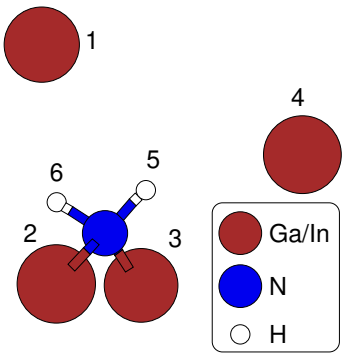

Figure 3. Schematic geometry of the C_{2v}+2 complex .

Table II. Atomic distances, d(X-Y), between the X and Y atoms involved in the C_{2v}+2 complex, whose geometry is schematized in Fig. 3. In the Table, the numbers in parentheses identify the cations shown in Fig. 3. The two H atoms neighboring the N atom are numbered as indicated in the same figure. The labels of the columns indicate in which alloy or N environment the complex is formed, e.g., GaAsN or the 4Ga N environment in InGaAsN. The bottom row reports the values of the CT-N distance (CT stands for a Ga or In cation) in the alloys without H. All distances are given in Å.

	GaAsN	4Ga	4In	InAsN
d(N-(2))	2.04	2.05	2.22	2.25
d(N-(3))	2.04	2.05	2.23	2.25
d(N-H5)	1.02	1.01	1.01	1.02
d(N-H6)	1.01	1.02	1.01	1.02
d(H5-(4))	2.65	2.66	2.88	2.90
d(H6-(1))	2.78	2.79	2.68	3.10
Pristine materials				
CT-N	2.06	2.07	2.20	2.23

Table III. The difference in total energy, ΔE, between the reaction products and the reacting species is also reported in the Table. It has to be taken into account that this difference is calculated from the total energies of the supercells containing a reacting species or a reaction product. These supercells are indicated in the schematized reactions. Thus, for instance, the reaction between an N atom in the 4Ga environment and a $H_{bc}(+)$ bonded to an As atom in the alloy lattice is represented by:

InGaAsN + (InGaAsN)As-$H_{bc}(+)$ ⟶ (InGaAs)-(4Ga)N-$H_{bc}(+)$ + InGaAsN (-1.49 eV)

where InGaAsN represents the supercell containing the N atom in the 4Ga-N cluster, (InGaAsN)As-$H_{bc}(+)$ the supercell containing an N atom (in a 4Ga-N cluster) and the As-$H_{bc}(+)$ complex. These are the reacting species. The reaction products come from a sort of migration of the H+ from the latter to the former supercell. Thus, the reaction leads to a supercell containing the N-$H_{bc}(+)$ complex, (InGaAs)-(4Ga)N-$H_{bc}(+)$, and a supercell containing one 4Ga-N cluster, InGaAsN. In this particular case, the supercells corresponding to a reacting species and a reaction product are identical and their total energies cancel each other in the ΔE difference (reported in parentheses in the above reaction). Negative ΔE values correspond to exothermic reactions. Thus, there is an energy gain when a H+ binds to N instead of As, as expected.

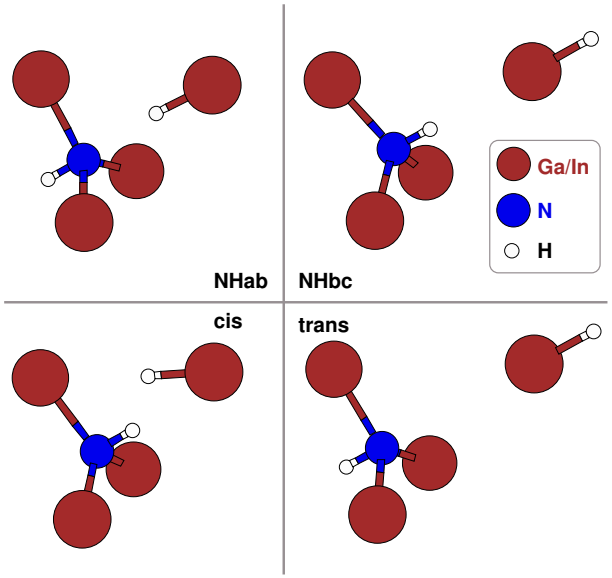

Figure 4. Schematic geometry of the investigated H_2^* complexes.

The results in Table III show that N-$H_{bc}(+)$ and C_{2v}+2 complexes always form with exothermic reactions in contrast to the positively charged H_2^* complexes, whose geometries are described in the following Section.

III. FORMATION ENERGIES OF H_2^* COMPLEXES

As mentioned in the main text, different H_2^* complexes were investigated both in their neutral and charged states. The geometries of the complexes investigated in addition to the H_2^*ab one, discussed in the main text, are shown in Fig. 4 together with the corresponding short labels, e.g., the Ga(or In)-H_{bc}-N-H_{bc} is referred to as H_2^*cis complex.

The formation energies H_f of the above H_2^* complexes formed by involving the 4Ga-N and 4In-N environments, as a function of the Fermi level, are shown in the upper and bottom panels of Fig. 5, respectively. In both N environments, the H_2^*ab complex gets the lower formation energy in the energy gap range, both in the neutral and charged states, albeit with H_f values close to those of the H_2^*cis complex in the case of the 4Ga-N environment.

As discussed in the main text, all of the di-hydrogen complexes, H_2^* and C_{2v}, can initially form only the the +2 charge state due to the shallow donor behavior of both the N-H and As-H complexes. Figure 3 in the main text shows that, in this charge state, the C_{2v} complex has the lowest formation energy in the whole energy gap range

Table III. Formation reactions of the investigated N-H complexes. The difference in total energy, ΔE, between the reaction products and the reacting species is given in eV.

N-H_{bc}(+) and C_{2v}+2 complexes	ΔE (eV)
InGaAsN + (InGaAsN)As-H_{bc}(+) ⟶ (InGaAs)-(4Ga)N-H_{bc}(+) + InGaAsN	-1.49
InGaAsN + (InGaAsN)As-H_{bc}(+) ⟶ (InGaAs)-(4In)N-H_{bc}(+) + InGaAsN	-1.14
(InGaAs)-(4Ga)N-H_{bc}(+) + (InGaAsN)As-H_{bc}(+) ⟶ (InGaAs)-(4Ga)C_{2v}+2 + InGaAsN	-1.27
(InGaAs)-(4In)N-H_{bc}(+) + (InGaAsN)As-H_{bc}(+) ⟶ (InGaAs)-(4In)C_{2v}+2 + InGaAsN	-1.06
H_2^*+2 complexes:	
(InGaAs)-(4Ga)N-H_{bc}(+) + (InGaAsN)As-H_{bc}(+) ⟶ (InGaAs)-(4Ga)H_2^*ab+2 + InGaAsN	0.64
(InGaAs)-(4In)N-H_{bc}(+) + (InGaAsN)As-H_{bc}(+) ⟶ (InGaAs)-(4In)H_2^*ab+2 + InGaAsN	0.94
(InGaAs)-(4Ga)N-H_{bc}(+) + (InGaAsN)As-H_{bc}(+) ⟶ (InGaAs)-(4Ga)H_2^*bc+2 + InGaAsN	0.92
(InGaAs)-(4In)N-H_{bc}(+) + (InGaAsN)As-H_{bc}(+) ⟶ (InGaAs)-(4In)H_2^*bc+2 + InGaAsN	1.33
(InGaAs)-(4Ga)N-H_{bc}(+) + (InGaAsN)As-H_{bc}(+) ⟶ (InGaAs)-(4Ga)H_2^*cis+2 + InGaAsN	0.65
(InGaAs)-(4In)N-H_{bc}(+) + (InGaAsN)As-H_{bc}(+) ⟶ (InGaAs)-(4In)H_2^*cis+2 + InGaAsN	1.19
(InGaAs)-(4Ga)N-H_{bc}(+) + (InGaAsN)As-H_{bc}(+) ⟶ (InGaAs)-(4Ga)H_2^*trans+2 + InGaAsN	1.49
(InGaAs)-(4In)N-H_{bc}(+) + (InGaAsN)As-H_{bc}(+) ⟶ (InGaAs)-(4In)H_2^*trans+2 + InGaAsN	1.77

with respect to the H_2^*ab complex. Thus, the same result holds for all of the charged H_2^* complexes. Moreover, as discussed above, only the C_{2v}+2 complex forms with exothermic reactions. All together, these results rule out the formation of H_2^* complexes. Finally, let us note that the indication given by the present results about a shallow donor behavior of the N-H, As-H, and C_{2v} complexes fully agrees with the experimental findings.[4] This contrasts with the behavior of all of the H_2^* complexes, which are always stable in their neutral state, as shown by the H_f values of Fig. 5.

IV. COMPARISON OF EXPERIMENTAL AND THEORETICAL BAND GAP ENERGIES.

The DFT-HSE band gap energies reported in Table II of the main text were calculated by using "extreme" as-grown and annealed InGaAsN alloy models. These models were simulated with supercells containing only one 4Ga-N or one 4In-N cluster, in order to simulate a predominance of a Ga-rich or an In-rich N environment, respectively. This is a severe, but inevitable, approximation. The simultaneous presence of both 4Ga-N and 4In-N clusters as well as of both N-H_{bc}(+) and C_{2v}+2 complexes would require indeed very large supercells and huge computational resources when they had to be used in DFT-HSE simulations (see also the above Section I). The above approximation limits the comparison of the theoretical results with the experiment to a qualitative level. However, it has to be considered that the efforts to get a more accurate comparison would be, in any case, affected by the absence of experimental data on the relative concentrations of the 4Ga-N and 4In-N environments in the annealed samples. Let us also recall that (as discussed in the main text), already at a qualitative level, the results of Table II in the main text accurately indicate an increase of the energy gap of the annealed alloy with respect the as-grown one, in agreement with the experiment, and give useful indications to explain the experimental findings.

Nevertheless, we attempted to refine the "rough" results of Table II of the main text in order to take into account the different distribution of Ga and In atoms in the as grown and annealed InGaAsN alloys, suggested by the experiments, as well as the different concentrations of the N-H_{bc}(+) and C_{2v}+2 complexes in the two alloys, suggested by the theoretical results. Such an attempt was performed, within the Vegard approximation, in two steps. First, it was taken into account that Ga-rich and In-rich N environments are both present, in different ratios, in the real as-grown and annealed alloys. In the case of the as-grown alloy, the band gap estimate was corrected by applying the Vegard approximation to an ideal mix of the 4Ga-N and 4In-N extreme alloy models and weighting the corresponding energy gaps with the 0.80/0.20 ratio approaching the $In_{0.21}Ga_{0.79}As_{0.975}N_{0.025}$ stoichiometry. In this way, from the 0.80x0.66+0.20x0.81 expression, see the present Table IV, a gap of 0.69 eV was estimated for a refined, as-grown (AG) alloy model. In the case of the annealed alloy, we used the indication given by the experimental results, see Table I in the main text, which show an increase of about a 9% of the energy gap in the sample annealed at 750° C (taken here as a reference point). More specifically, we estimated the weights which have to be assigned to the 4Ga-N and 4In-N gaps of the extreme models in order to achieve, in the Vegard approximation, an identical increase of the energy gap with respect to the AG value. We found the values of 0.37 and 0.63, respectively, which lead to the 0.37x0.66+0.63x0.81 expression and to the value of 0.75 eV for the energy gap of a refined, annealed (ANN) alloy model. These refined energy gaps, estimated for the alloys without hydrogen, are reported in the first row of the present Table IV together with those estimated for the extreme alloy models (taken from the Table II in the main text).

In a second step, we took into account both the ratios between the Ga-rich and In-rich N environments in the AG and ANN alloys and the ratios between the concentrations of the two complexes [N-H_{bc}(+)]/[C_{2v}+2] estimated in the cases of the 4In-N clusters and 4Ga-N clus-

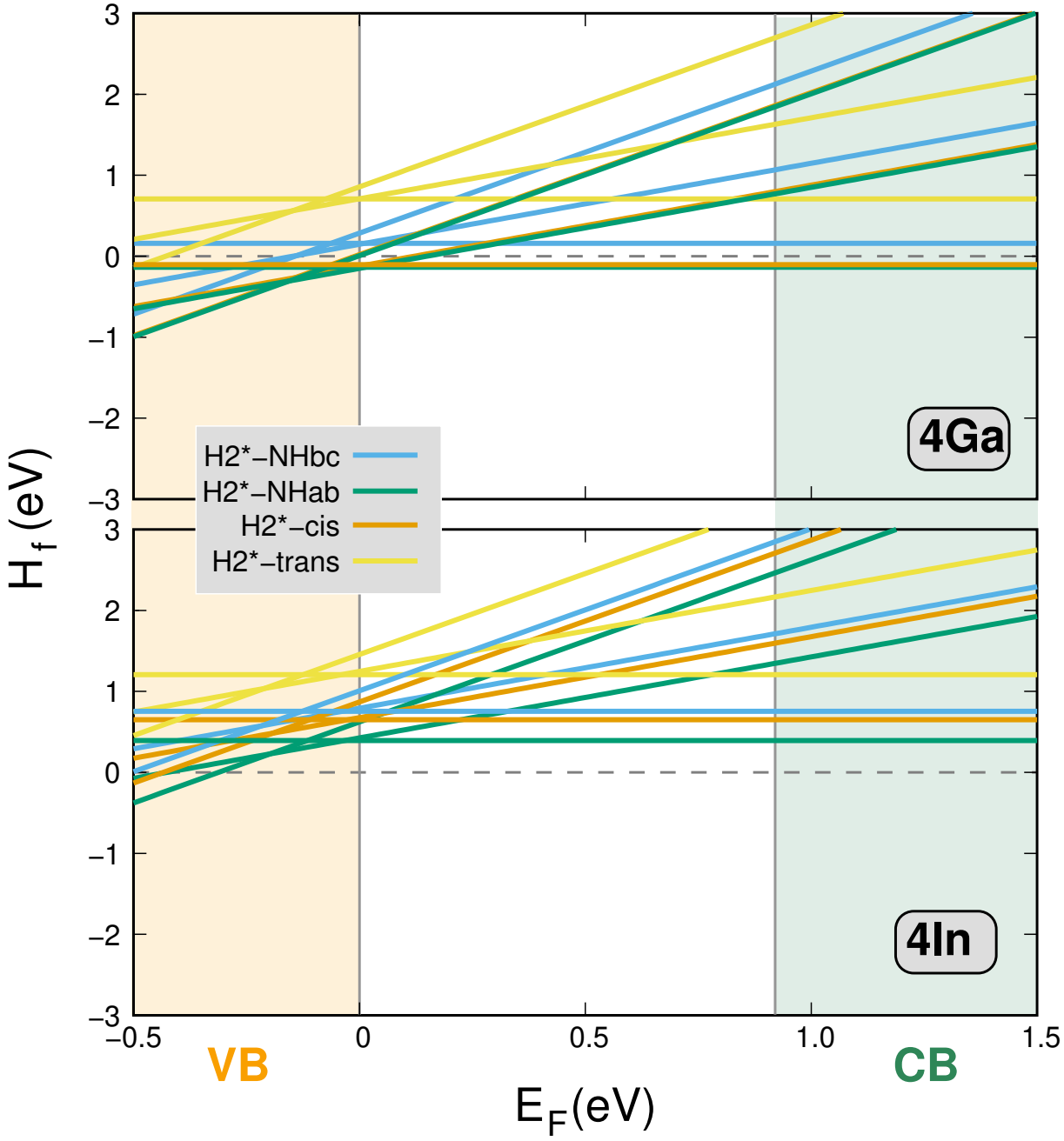

Figure 5. Formation energies (H_f) as a function of the Fermi level E_F for H_2^* complexes forming in the 4Ga-N and 4In-N clusters are shown in the upper and bottom panels of the figure, respectively. E_F values are taken in the range 0.0 eV - 0.92 eV, whose limits correspond to the top of the valence band (VB) and the bottom of the conduction band (CB), respectively. This range also corresponds to the estimated, partially recovered InGaAs energy gap (see the Theoretical Methods Section in the main text).

ters, which are equal to 4×10^3 and ≈ 7, respectively. We recall that, based on these results, we assumed a coexistence of the two complexes in equal percentages in the Ga-rich N environment, replaced by a total predominance of the N-$H_{bc}(+)$ complex in the case of the In-rich environment. Then, in the case of the as-grown alloy, still in the Vegard approximation, we used the energy gaps induced by the formation of each complex with a 4Ga-N or a 4In-N cluster (given in Table II of the main text and reported in the second row of present Table IV) in the expression [0.80x(0.5x0.86 + 0.5x1.04) + 0.20x(1.0x0.93)] = 0.95 eV, where equal weights of 0.5 were used for the energy gaps induced by each complex in the 4Ga-N case, while a weight equal 1.0 was considered for the energy gap induced by the dominating $H_{bc}(+)$ complex, in the 4In-N case. Similarly, in the case of the annealed model,

we used the expression [0.37x(0.5x0.86 + 0.5x1.04) + 0.63x(1.0x0.93)] = 0.93 eV, see present Table IV.

The above estimates of the energy gaps are reported in Table IV together with the values of the energy gap differences, ΔEg, and of the ΔEg/Eg ratios, for a comparison with the corresponding experimental values in Table I of the main text. Some of these experimental results are also reported in Table IV.

A comparison of the experimental and refined theoretical results shows that: i) in the case of the $In_{0.25}Ga_{0.75}As_{0.985}N_{0.015}$ as-grown alloy, hydrogen increases the energy gap up to 1.115 eV, by recovering about a 91% of the $In_{0.25}Ga_{0.75}As$ energy gap, 1.220 eV (values taken from the Fig. 1 in the main text). The theoretical results achieved for the as-grown InGaAsN model show an increase of the energy gap up to 0.95 eV against the value of 1.01 eV estimated for the InGaAs energy gap, corresponding to a recovering of 94%; ii) experimentally, the annealing of the InGaAsN samples induces an increase of the energy gap that is reproduced by both the rough data of the extreme alloy models and the refined data reported in Table IV; iii) the gap recovered by H in the as-grown sample, 1.231 eV, decreases to the value of 1.163 eV for the sample annealed at 750° C. This corresponds to a reduction of 6% against a 2% given by the corresponding 0.95 eV and 0.93 eV theoretical values; iv) the comparison of theoretical and experimental ΔEg/Eg values gives 38% vs 32% for the as-grown alloy and 24% vs 14% for the alloy annealed at 750° C.

Thus, just applying the Vegard approximation, it is possible to achieve a satisfactory, quantitative agreement of the refined theoretical results with the experimental ones.

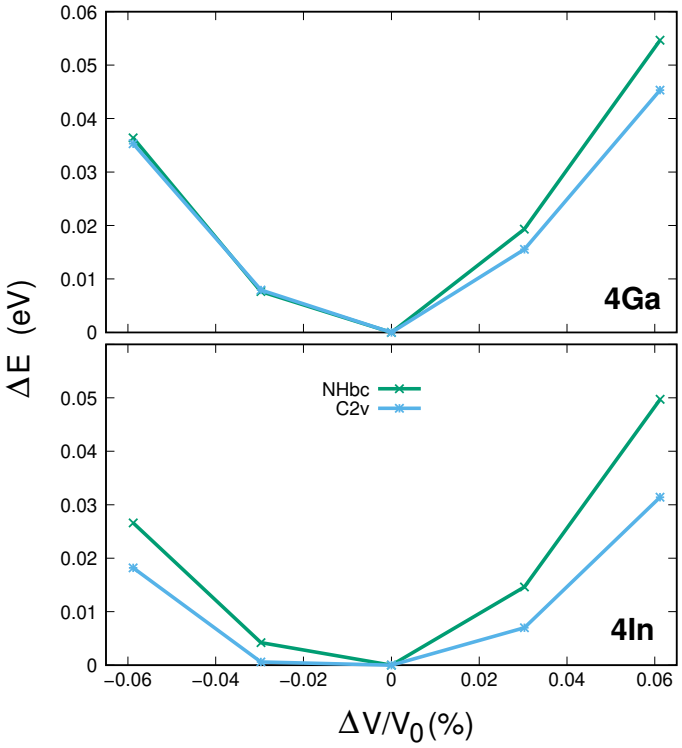

Figure 6. Changes of the total energy difference ΔE = E-E_0, where E_0 is the total energy corresponding to the equilibrium geometry, as a function of changes of the N-tetrahedron volume V with respect to V_0 (the volume corresponding to the equilibrium geometry) are shown in the figure for the N-H_{bc}(+) and C_{2v}+2 complexes forming in the 4Ga-N environment (upper panel) and in the 4In-N environment (bottom panel).

V. SELECTIVE EFFECTS OF THE HOST MATRIX.

In the main text, mostly qualitative arguments were used to justify the existence of a selective effect exerted by the InGaAsN host matrix on the formation of the N-H_{bc}(+) and C_{2v}+2 complexes. In detail, for N-H complexes forming in the 4In-N environment, *and only in this environment*, such an effect favors the formation of the N-H_{bc}(+) complex and hinders that of the C_{2v}+2 one.

In order to give further support to the existence of this host-matrix effect, we calculated for each complex formed in the 4In-N (4Ga-N) environment, the changes in the total energy induced by small expansions or contractions of the volume of the 4In (4Ga) tetrahedron surrounding the N atom (the tetrahedron sketched in Fig. 3 of the main text). In correspondence of each change of the tetrahedron volume, the supercell total energy was minimized by keeping fixed the tetrahedron vertexes and by allowing the atoms in the N-H or N-2H units as well as the other atoms in the simulation supercell to relax by minimizing the atomic forces.

Figure 6 shows, for a given X complex formed in the 4Ga-N or 4In-N environment, the changes of ΔE[X] = E - E_0, i.e., the total energy E referred to the total energy corresponding to the equilibrium geometry (E_0), as a function of the changes of the tetrahedron volume V with respect to V_0 (the volume corresponding to the equilibrium geometry). The graphs in the figure show that, in correspondence of a same percentage of volume expansion or contraction, the ΔE[N-H_{bc}(+)] and the ΔE[C_{2v}+2] values are much closer in the case of the 4Ga-N environment than in that of the 4In-N one. By considering that, in particular, the volume expansion mimics the complex formation, these results give a clear evidence of an opposition exerted by the surrounding matrix to the formation of the C_{2v}+2 complex with respect to the N-H_{bc}(+) complex, in the case of the 4In-N environment, much stronger than that occurring in the 4Ga-N case, thus fully supporting the arguments presented in the main text.

The origin of the effect exerted by the host InGaAs matrix is traced back to the two-component nature of this alloy, more specifically, to the different mechanical properties of its GaAs and InAs components. In fact, as mentioned in the main text, e.g., in the case of the N-H_{bc}(+) and C_{2v}+2 complexes forming in the 4In-N envi-

Table IV. The first row of the Table reports the band gap energies, E_g, calculated for the as grown (AG) and annealed (ANN) extreme InGaAsN models, containing only one 4Ga-N and one 4In-N cluster, respectively, and for the corresponding, refined models assuming the coexistence of the two N clusters (whose relative weights are indicated in parentheses). E_g values induced by the formation of N-H_{bc}(+) and C_{2v}+2 complexes alone or coexisting in the ratios indicated in parentheses are reported in the second row. Differences between the latter and the former E_g values, ΔE_g, and $\Delta E_g/E_g$ ratios are reported in the third and fourth row, respectively. For an easy comparison, some experimental results are also reported in parentheses.

	AG (4Ga-N)	ANN (4In-N)	AG (4Ga-N)	ANN (4In-N)	AG 4Ga-N/4In-N (0.80/0.20)	ANN 4Ga-N/4In-N (0.37/0.63)
	H_{bc}(+)	H_{bc}(+)	C_{2v}+2	C_{2v}+2	H_{bc}(+)/C_{2v}+2 (0.5/0.5)	H_{bc}(+)/C_{2v}+2 (1.0/0.0)
E_g - InGaAsN (eV)	0.66	0.81	0.66	0.81	0.69 (0.930)	0.75 (1.016)
E_g - InGaAsN + H (eV)	0.86	0.93	1.04	1.03	0.95 (1.231)	0.93 (1.163)
ΔE_g (eV)	0.20	0.12	0.38	0.22	0.26 (0.301)	0.18 (0.147)
$\Delta E_g/E_g$	30%	15%	57%	27%	38% (32%)	24% (14%)

ronment of the InGaAsN alloy, the two complexes form by expanding the corresponding N-tetrahedron against a *host* InGaAs matrix that has a smaller lattice constant and a larger bulk modulus (i.e., a larger stiffness) (5.68 Å and 74 GPa, respectively) than the *host* InAs matrix of InAsN (6.01 Å and 61.4 GPa, respectively). The reverse occurs in the case of complexes forming in the 4Ga-N environment, where they expand their N-tetrahedron favored by an InGaAs matrix having a larger lattice constant and a smaller bulk modulus than the *host* GaAs matrix of GaAsN (5.59 Å and 81.2 GPa, respectively).

* francesco.filippone@ism.cnr.it

[1] C. Peng, H. Liu, J. Konttinen, and M. Pessa, Journal of Crystal Growth **278**, 259 (2005), 13th International Conference on Molecular Beam Epitaxy.

[2] P. J. Klar, H. Grüning, J. Koch, S. Schäfer, K. Volz, W. Stolz, W. Heimbrodt, A. M. K. Saadi, A. Lindsay, and E. P. O'Reilly, Phys. Rev. B **64**, 121203 (2001).

[3] S. Kurtz, J. Webb, L. Gedvilas, D. Friedman, J. Geisz, J. Olson, R. King, D. Joslin, and N. Karam, Applied Physics Letters **78**, 748 (2001), https://doi.org/10.1063/1.1345819.

[4] H. P. Xin, C. W. Tu, and M. Geva, Journal of Vacuum Science & Technology B: Microelectronics and Nanometer Structures Processing, Measurement, and Phenomena **18**, 1476 (2000), https://avs.scitation.org/doi/pdf/10.1116/1.591407.